DESIGN AND CONSTRUCTION OF
A LOW SPEED WIND TUNNEL

By

Jonathan D. Jaramillo

A thesis submitted in partial fulfillment of the
requirements for the degree of

Bachelor of Science

Houghton College

May 2017

Signature of Author……..
Department of Physics
May 13, 2017

……..
Dr. Kurt Aikens
Assistant Professor of Physics
Research Supervisor

……..
Dr. Brandon Hoffman
Associate Professor of Physics

DESIGN AND CONSTRUCTION OF A LOW SPEED WIND TUNNEL

By

Jonathan Jaramillo

Submitted to the Department of Physics
on May 13th, 2017 in partial fulfillment of the
requirement for the degree of
Bachelor of Science

Abstract

Despite advances in computational aerodynamics, wind tunnels are and will continue to be a cornerstone in the design process for a wide range of vehicles. This mostly stems from the difficulties of accurately and efficiently predicting turbulent flowfields computationally. To expand in-house aerodynamics capabilities, a general-purpose low-speed wind tunnel is being designed and built in the Houghton College Physics Department. This wind tunnel is designed to reach test section speeds of up to 44.7 m/s (100 mph). To aid in the initial design, semi-empirical formulas are used to estimate aerodynamic efficiencies and the required fan-blower power as a function of various design choices. Tunnel geometry is selected to optimize test section air flow quality, test section size, and diffuser angle (to avoid boundary layer separation), while the overall tunnel size is constrained to fit in the allotted laboratory space. The proposed closed-circuit wind tunnel is vertically oriented to reduce footprint, and is 4.72 m (15.5 ft) long by 1.67 m (5.5 ft) by 0.762 m (2.5 ft) wide. The overall design is presented and current design and construction progress is highlighted. Additionally, future research studies that could utilize the wind tunnel are discussed.

Thesis Supervisor: Dr. Kurt Aikens
Title: Assistant Professor of Physics

TABLE OF CONTENTS

TABLE OF FIGURES

Chapter 1

BACKGROUND AND MOTIVATION

1.1. Approaches to Fluid Mechanics

Since the time of the Wright brothers, the need for reliable aerodynamic predictions has only increased. Demand from both military and private aeronautics sectors has driven rapid increases in flight technology. Similarly, the automotive, nautical, civil engineering, and many other industries have increased the demand for a comprehensive understanding of fluid flow around objects such as cars, ships and buildings. There are three techniques frequently used for solving aerodynamic design problems – theoretical, computational, and experimental – each having distinct advantages and disadvantages [1][2].

Theoretical methods refer to analytical approaches to solving the governing equations of fluid dynamics. The distinct advantage to analytical methods is that they result in closed-form solutions. The formulas obtained from an analytical approach can give a great deal of insight as to how the system will behave under different conditions. Unfortunately, analytical solutions are often impossible to obtain, except in cases where the governing equations are linear or can be approximated as such. One way to obtain linear governing equations is to consider only simple geometries, such as flow through an infinitely long pipe. That said, many problems of interest involve complex geometries such as cars or planes. However, theoretical approaches are useful for gaining intuition for how given flow fields will behave and understanding basic flow phenomena. Theoretical approaches also continue to play a vital role in validating computational methodologies. Because computational solutions are approximations, it is helpful to test the accuracy of computational algorithms on problems for which there are analytical solutions.

The second approach to the aeronautic design process is computational, often referred to as computational fluid dynamics (CFD). These methods use computer algorithms to approximate the solutions to the governing equations of fluid mechanics. For a given flow problem the geometry must be modeled using CAD. Initial and boundary conditions must

then be defined and the flow domain must be discretized into a grid. In many approaches, the solution is assumed to be constant in each cell and the governing equations are also discretized to model how each cell's solution changes. An example of a grid for an airfoil is shown in Figure 1. Once an algorithm is chosen, the simulation can be performed.

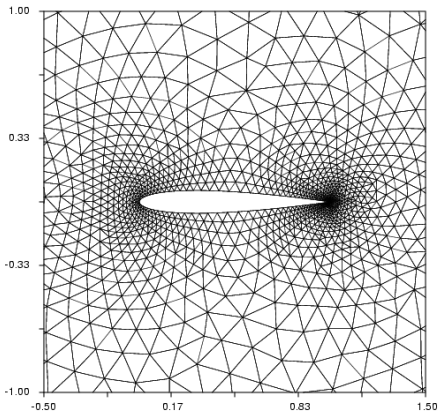

Figure 1. An example of a grid mesh for the NACA 0012 airfoil. Grid point density increases near the leading and trailing edge of the airfoil because the solution near these points varies greater with space and time. Figure taken from Ref. [3].

The field of CFD has seen tremendous growth in the past fifty years due to the continuous increase in computational power and memory of computers. The rate of computer evolution during the 1960's and 70's led some researchers to predict that computer simulations would eventually be able to more accurately analyze free flight scenarios than wind tunnels and would even replace them completely [4]. Unlike analytical methods, CFD has the capacity to model complex geometries and does not need approximations to be made to the governing equations of fluid mechanics to obtain solutions. This means that few physical assumptions need to be made to find a solution. CFD can also obtain time-resolved flow solutions for any problem. Depending on the methodologies chosen, it is feasible to perform viscous simulations on a full aircraft in less than a day using a personal computer [5]. Furthermore, there are problems for which experimental data is difficult or impossible to obtain. For example, taking measurements inside of a jet engine is not often practical. For this reason, CFD is an indispensable engineering tool that can dramatically reduce the amount of experimental testing needed in an aerodynamic design process.

Despite the many advantages of CFD, there are some disadvantages that inhibit CFD from completely replacing wind tunnel testing. Like any field that relies on numerical methods, CFD is subject to truncation errors in floating point calculations. Round-off error is introduced in CFD because computers hold a finite number of digits in arithmetic operations. This error is proportional to the number of grid points. CFD also introduces discretization error. Discretization error is defined as the difference between the partial differential equation solution and the discretized approximation to the differential equation solution when round-off error is excluded [2]. Additionally, it might seem as though solutions to increasingly complicated problems can be found more easily with advances in computational power. However, this is not necessarily the case. This is due to difficulties in software parallelization. It is also important to point out that while CFD can predict aerodynamic performance with increasing accuracy, engineers are often interested in other features such as reliability, operability, and maintainability. For example, CFD alone cannot predict if an engine can restart at cruising speed, or how many flight hours can be achieved before service is needed.

Another difficulty associated with CFD is that of turbulence modeling. One approach to modeling fluid flow is called Direct Numerical Simulation (DNS) simulations. This method does not make approximations to the governing equations but often requires orders of magnitude more mesh points than a computationally cheaper alternative such as Reynolds-Averaged Navier-Stokes (RANS) [4] [6]. Because of its computational cost, DNS is almost exclusively used for theoretical analyses. While DNS can be used to study more problems as computational power increases, its application to most practical engineering problems remains in the distant future. Alternatively, RANS is one of the most common CFD methods used in engineering. It relies on statistically averaging the Navier-Stokes equations in time. While RANS methods can be used for cases of mild separation, they often are not as capable in cases of massively separated flows [5]. Another approach to CFD is called large-eddy simulation (LES). LES is like RANS in that it makes assumptions that result in approximations to the Navier-Stokes equations. However, instead of averaging the Navier-Stokes equations, it filters the Navier-Stokes equations, removing high wave-number components [7]. The computational cost and accuracy of this method falls between RANS

and DNS. Figure 2 shows the relationship between computational cost and the number of assumptions associated with each model. It should be stated that despite these shortcomings and those discussed previously, CFD has proven to be an invaluable tool in the aerodynamic design process, dramatically reducing the number of design cycle iterations needed in the design process.

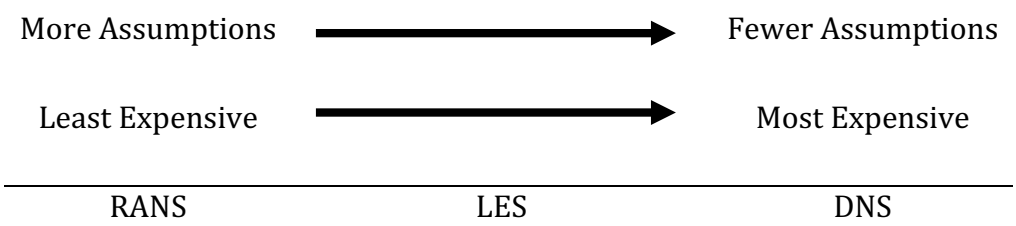

Figure 2. A diagram of the relative accuracy and cost of various CFD methods.

The third approach to obtaining aerodynamic predictions is experimental. Historically, wind tunnel testing has been used as the basis for the design process of all contemporary flying vehicles, starting at the time of the Wright brothers. Regardless of the fact that the number of military aircraft programs has shown a downward trend since the 1950's, the number of wind tunnel test hours per program has been on a steady rise [8]. This can be attributed to the fact that as aircraft become more advanced, the amount of testing needed to perfect a given design increases. Historical trends show that the amount of experimentally acquired data for an aircraft program have been and will continue to grow. Wind tunnels, however, are not without their limitations. For example, the cost to build and maintain a wind tunnel varies depending on its size and features, but it is rarely a cheap endeavor. This is because wind tunnels can take years and countless man-hours to design and build. Making accurate models with properly calibrated equipment is a difficult process and only increases the operating costs of a wind tunnel. The main challenge associated with wind tunnel testing is properly replicating flow parameters. For low speeds, this involves building a model of the object of interest and replicating the desired Reynolds number. Achieving high Reynolds numbers in tests can often prove to be difficult without expensive infrastructure, and in some cases the desired Reynolds number cannot be experimentally achieved at all. Furthermore, care must be taken to avoid measurement inaccuracies

related to the proximity of the tunnel walls to the test object [9]. The fact remains that despite growths in computational methodologies, CFD has not, and will not completely replace experimental methodologies for the foreseeable future in solving aerodynamic design problems [1].

1.2. History of Experimental Aerodynamics

The modern concept of a wind tunnel has only been around for 150 years. Prior to wind tunnels the most systematic approach to experimental fluid dynamics involved attaching a model to the end of a whirling arm. Benjamin Robins (1707 – 1751) is attributed with employing the first whirling arm mechanism and he used it to make large advancements in our early understanding of fluid mechanics [10]. Figure 3 is a sketch of Robins' whirling arm mechanism. It was not until Sir George Cayley (1773-1857), who also used a whirling arm mechanism, began his work that experimental aerodynamics would contribute the vital test data needed to design what is believed to be the first recorded heavier-than-air vehicle in history [10]. Cayley's first successful unmanned glider had a wing span of 200 square feet. By 1852 he made a triplane that integrated many concepts of modern planes: fixed wings, fuselage and tail. Cayley was the first to conceptually separate the mechanisms behind lift and thrust. Prior to Cayley, most designs for flying machines incorporated one mechanism for both lift and propulsion: ornithopters that flapped mechanical wings [10, 11]. With this flying mechanism paradigm shift came the need for a better way to experimentally measure forces such as lift and drag. Frank H. Wenham (1824-1908) is frequently credited with designing and building the first wind tunnel [10]. As a council member of the Aeronautical Society of Great Britain, he received funding to design an apparatus that pulled air through a 3.66 m (12 ft) tube past a model using a steam-engine-powered fan blower.

While the years after the creation of the first wind tunnel (1871) were full of ground breaking experiments performed by Wenham and his colleagues, the question remained: did experimental results obtained with a scale model bear any resemblance to those of a full-sized aircraft [10]? It was not until 1885 that Osborne Reynolds showed that the flow patterns over a scale model would be same for a full-scale model if a certain parameter is

the same in both experiments [12]. This parameter, which will be discussed later, is now known as the Reynolds number. The significance of this discovery is that wind tunnels could be used to generate meaningful experimental results for full-scale models by completing testing on scale models if the Reynolds number is properly replicated. Another fifteen years would pass before Wilbur and Orville Wright, frustrated with the accepted aerodynamic design tables of their day, would use results from their own wind tunnel to build the world's first powered, manned, heavier-than-air flying vehicle [11,10]. A sketch of the Wright brothers' wind tunnel is shown in Figure 4.

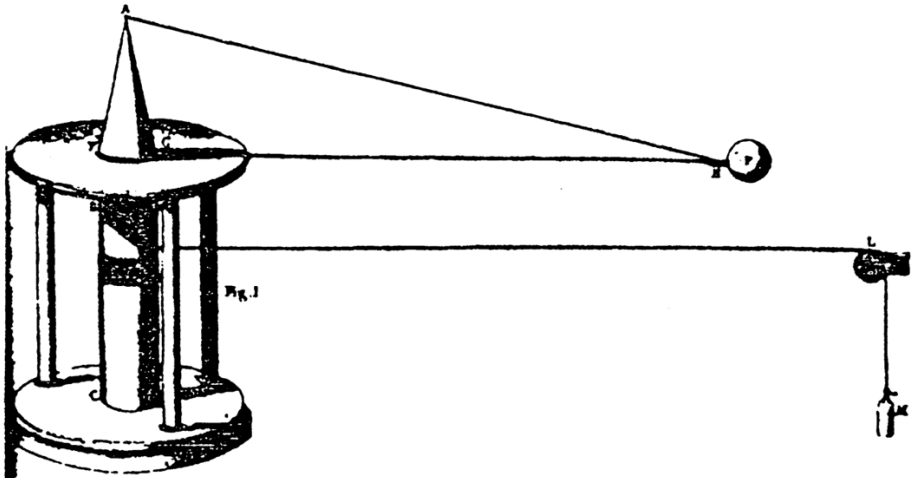

Figure 3. A sketch of Benjamin Robin's whirling arm. A string is wrapped around a cylinder and a mass is tied to the other end (bottom right). The string is passed over a pulley and the cylinder and attached arm rotate as the mass falls. The model of interest is attached to the end of the arm. Image taken from Ref. [13].

Since the early development of the modern wind tunnel, a variety of different wind tunnels have been developed for many special purposes. These include the NACA variable density tunnel, which was capable of performing experiments at high Reynolds numbers [14] and the wind tunnel at the NASA Ames Research Center, with a 40 by 80-foot test section for full-scale testing [15]. Further examples of specialized wind tunnel applications include vertical and/or short landing and takeoff vehicle (V/STOL) testing and acoustic testing. For more examples of more recent specialized tunnels and applications, see Barlow [1].

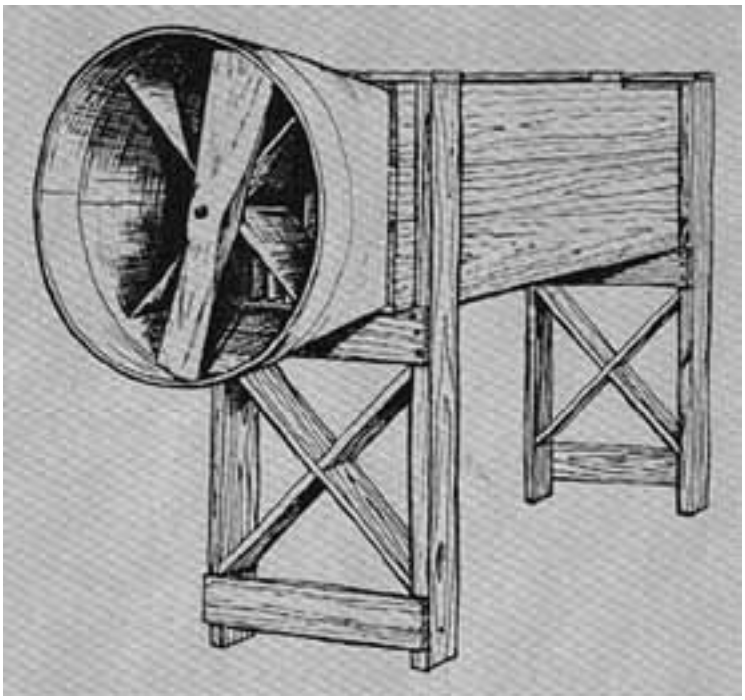

Figure 4. A sketch of the Wright brothers' wind tunnel used to design the first heavier-than-air powered flight vehicle. The fan was belt driven and powered by a small gas engine the Wright brothers used for powering machinery in their bike shop. The air was pushed through the tunnel by the fan and, as a result, the Wright brothers struggled to find a way to straighten the swirling motion of the air as it passed the model. Image taken from Ref. [10].

1.3. Objective

As mentioned before, analytical and computational approaches to aerodynamic design problems are not always sufficient. As a result, Houghton has started a design project to build a new general-purpose low-speed wind tunnel to expand its in-house aerodynamic testing capabilities. This wind tunnel will give Houghton the ability to perform a wide range of experiments. Specific examples include tests on plasma actuators for flow control and tests on aircraft models with ice buildup. Plans for future research will be discussed later. Furthermore, a general-purpose wind tunnel will give Houghton the ability to perform a variety of laboratory activities as part of a fluid dynamics course.

This thesis discusses the overall design of the wind tunnel and the design process used. The flow velocity throughout the tunnel was estimated using a quasi-one-dimensional

assumption. Given the velocity, semi-empirical equations were used to predict the tunnel efficiency based on the air properties (e.g., test section speed and viscosity) and sizing choices. An Octave script was written to automate the calculations for a variety of design choices and estimate fan power requirements for each. Once construction of the wind tunnel is complete, this will provide another opportunity for research: testing the utilized design process. Are the estimated section losses and overall power estimates comparable to those measured in the wind tunnel? These results could be valuable to those seeking to design and build similar wind tunnels in the future.

The remainder of this work is as follows. Chapter 2 describes the theory of fluid mechanics and concepts behind wind tunnel design. This includes the Navier-Stokes equations, quasi-one-dimensional flow, semi-empirical component efficiency equations, and measurement techniques. Chapter 3 describes the specific design process used along with explanations of design choices made. Furthermore, Chapter 3 covers the design and construction progress made thus far. Lastly, Chapter 4 covers future work and possible experiments in more depth.

Chapter 2

THEORY

2.1. Fluid Mechanics

2.1.1. Theoretical Development

There are three fundamental principles which govern fluid mechanics. These are conservation of mass, Newton's second law of motion, and conservation of energy. These three principles result in equations which relate various quantities (e.g. pressure, density, velocity) as they vary in time and space. Only a brief overview of these equations will be presented. For a more in-depth development see Anderson [11] or Currie [16].

First, consider the equation which follows from the principle of conservation of mass. It can be written as

$$\frac{\partial \rho^*}{\partial t^*} + \frac{\partial (\rho^* u_i^*)}{\partial x_i^*} = 0 \qquad (1)$$

where ρ is the fluid density, $\boldsymbol{u}$ is the vector fluid velocity, t is the time, $\boldsymbol{x}$ is the vector of spatial coordinates, and a superscript asterisk indicates dimensional quantities. Equation (1) is often referred to as the continuity equation [2].

The second governing equation of fluid mechanics comes from the principle of conservation of momentum, which is an application of Newton's second law of motion to an element of the fluid. The two types of forces that act on a fluid element are body forces, such as gravitational and electromagnetic forces, and surface forces, such as pressure and viscous forces. In many aerodynamic problems body forces are insignificant. Therefore, they are neglected. The resulting equations are given by

$$\frac{\partial (\rho^* u_j^*)}{\partial t^*} + \frac{\partial \left(\rho^* u_j^* u_k^*\right)}{\partial x_k^*} = \frac{\partial}{\partial x_i^*}\left\{-p^* \delta_{ij} + \mu^* \left(\frac{\partial u_i^*}{\partial x_j^*} + \frac{\partial u_j^*}{\partial x_i^*} - \delta_{ij} \frac{2}{3} \frac{\partial u_k^*}{\partial x_k^*}\right)\right\} \qquad (2)$$

where p is the pressure and μ is the viscosity. Equation (2) is a vector equation indicated by the free index, j.

The last equation of fluid mechanics comes from conservation of energy. Conservation of energy states that the change in total energy (internal plus kinetic) is equal to the sum of the total work done on the system and any energy transferred by thermal conduction. This equation is given by

$$\frac{\partial}{\partial t^*}\left(\rho^* e^* + \frac{1}{2}\rho^* u_j^* u^*{}_j\right) + \frac{\partial}{\partial x_k^*}\left[\left(\rho^* e^* + \frac{1}{2}\rho^* u_j^* u_j^*\right) u_k^*\right] = \frac{\partial}{\partial x_i^*}\left\{u_j^*\left(-p^*\delta_{ij} + \mu^*\left[\frac{\partial u_i^*}{\partial x_j^*} + \frac{\partial u_j^*}{\partial x_i^*} - \delta_{ij}\frac{2}{3}\frac{\partial u_k^*}{\partial x_k^*}\right] + \delta_{ij}k^*\frac{\partial T^*}{\partial x_j^*}\right)\right\} \tag{3}$$

where k is the thermal conductivity, e is the internal energy and T is the temperature. It is important to note that only five equations have been given, but there are seven unknowns: density, pressure, temperature, internal energy, and three velocity components. To solve these equations two more algebraic expressions for pressure and internal energy should be used. They are given by

$$p^* = \rho^* R^* T^* \tag{4}$$

and

$$e^* = c_v^* T^* \tag{5}$$

where Equation (4) is the ideal gas law and Equation (5) is an expression for the internal energy in terms of temperature and specific heat at constant volume, c_v. In this case, R is the specific gas constant, which has a value of 287 $Jkg^{-1}K^{-1}$ for air. These two equations are often substituted into the energy equation to give five equations with five unknowns. Together, these five equations are known as the Navier-Stokes equations.

2.1.2. Quasi-One-Dimensional Flow

A thorough treatment of quasi-one-dimensional flow is given by Anderson [11] and a similar approach to his is used here. When considering the air flow through a wind tunnel,

one approach is to use the Navier-Stokes equations to model the flow in three dimensions. However, no analytical solution exists and CFD would take time and computational resources. A more economic approach exists. In wind tunnels, the cross-sectional area, A, varies only as a function of the length along the loop of the tunnel, x, meaning $A = A(x)$. For fluid mechanics problems involving ducts, such as estimating wind tunnel efficiency, it may be reasonable to assume that the flow field properties are uniform across any cross section, and hence only vary as a function of x. This assumption is valid in cases where the flow is assumed to be steady, i.e., no time-dependence. Furthermore, it is assumed that the boundary layers along the surface are very thin, and that changes in area with respect to x are small. If changes in area with respect to x are small, then the z and y components of the velocity are small, allowing the fluid motion to be treated as though it is only in the x direction. A flow that approximately meets these requirements is referred to as a quasi-one-dimensional flow. Although quasi-one-dimensional flow is only an approximation of the time-dependent three-dimensional flow that is really occurring in the wind tunnel, the results are sufficiently accurate for use in estimating the efficiency of the wind tunnel.

The main result needed for the present work is the incompressible quasi-one-dimensional flow version of the continuity equation which comes from Equation (1). Using the divergence theorem and assuming a time-independent flow, the integral form of the continuity equation is

$$\oiint_S \rho \vec{u} \cdot d\vec{s} = 0 \tag{6}$$

where S is the the surface that bounds a given volume of fluid. This equation can be applied to a duct like the one shown in Figure 5. The fluid in the duct is bounded by cross-sectional area A_1 on the left, A_2 on the right, and the walls of the duct itself. In this case, Equation (6) can be written as

$$\iint_{A_1} \rho \vec{u} \cdot d\vec{s} + \iint_{A_2} \rho \vec{u} \cdot d\vec{s} + \iint_{wall} \rho \vec{u} \cdot d\vec{s} = 0. \tag{7}$$

The last term describes the fluid flow that passes through the wall, which is zero. Because $d\vec{s}$ points out of the volume, and x-velocity, u, and density are assumed to only vary with x, the remaining terms can be written as

$$\iint_{A_1} \rho\vec{u} \cdot d\vec{s} = -\rho_1 A_1 u_1 \tag{8}$$

and

$$\iint_{A_2} \rho\vec{u} \cdot d\vec{s} = \rho_2 A_2 u_2 \, . \tag{9}$$

Therefore, from Equation (7),

$$\rho_1 A_1 u_1 = \rho_2 A_2 u_2 \, . \tag{10}$$

Equation (10) is the quasi-one-dimensional continuity equation. It is a statement of conservation of mass and that mass flow through a duct is constant. In the case of an incompressible flow where ρ is constant,

$$A_1 u_1 = A_2 u_2 \, . \tag{11}$$

For air flow at Mach numbers less than 0.3, the density varies by less than 5%. Therefore, the incompressible assumption is made in the design of this low-speed wind tunnel.

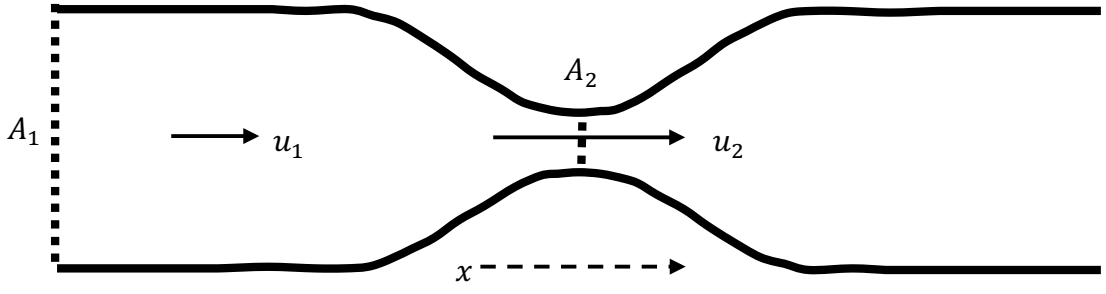

Figure 5. Quasi-one-dimensional flow through a duct. The dashed lines bound the fluid volume of interest. In the case of incompressible flow, the area and velocity are related by Equation (11).

2.1.3. Bernoulli's Principle

Bernoulli's principle is a statement of conservation of energy. It mathematically expresses the idea that the sum of all forms of energy along a streamline must be the same at all points. That is,

$$\frac{1}{2}\rho u^2 + \rho g z + p = \text{constant} \tag{12}$$

where g is the acceleration due to gravity, z is the elevation of the fluid, p is the static pressure, u is the fluid velocity, and ρ is the fluid density. The first term, $\frac{1}{2}\rho u^2$, is referred to as the dynamic pressure, and expresses the kinetic energy of the fluid. The second term, $\rho g z$, describes the gravitational potential energy of the fluid. The last term, p, is the static pressure of the system and can be thought of as a measure of internal energy of the system. This expression of conservation of energy is only valid under a certain set of assumptions. The first assumption is that the fluid is incompressible – the density is constant. Secondly, the flow is steady and does not change with time. The last assumption is that viscous forces are negligible.

When considering wind tunnel design, the change in gravitational potential energy of the fluid is small compared to that of the dynamic and static pressures. As a result, this term is often neglected. The stagnation pressure, p_0, is defined as the sum of the static and dynamic pressures

$$p_0 = \frac{1}{2}\rho u^2 + p\,. \tag{13}$$

The stagnation pressure of a system is constant under the same set of assumptions as Bernoulli's principle. Energy, however, is not conserved in a non-ideal system. For example, viscous forces are not negligible throughout the wind tunnel. Therefore, inefficiencies throughout the tunnel can be expressed as a drop in stagnation pressure. This idea is fundamental to the wind tunnel design process and is discussed in greater detail in Section 2.2.3.

2.2. Wind Tunnels

In this section, the Navier-Stokes equations are presented in non-dimensional form to highlight the important parameters for wind tunnel applications. Section 2.2.2 covers some basic design features of wind tunnels and gives some examples of operational wind tunnels with these features. Next, Section 2.2.3 discusses the process and equations by which power estimates are made for wind tunnel design. Lastly, Sections 2.2.4 and 2.2.5 discuss options for fan selection and other considerations for construction of a wind tunnel.

2.2.1. Important Parameters

Wind tunnel testing is most often completed on scale models in an effort to better understand flow fields around a full-scale object. How does one know if flow fields around a scale model are similar to flow fields around a full-scale object? Anderson [2] defines two flows to be dynamically similar if:

1) The streamline patterns are geometrically similar.

2) The distributions of $\frac{u^*}{u_r^*}, \frac{p^*}{p_r^*}, \frac{T^*}{T_r^*}$, etc., where subscript r denotes a reference quantity, are the same when plotted against coordinates non-dimensionalized by a common reference length.

3) The resulting non-dimensionalized forces (e.g. lift, drag) are the same.

In general, flow solutions are a function of all of the parameters included in the dimensional Navier-Stokes equations. However, the Buckingham Pi theorem [17] states that the number of free parameters in the Navier-Stokes equations can be reduced to three. To do this, the Navier-Stokes equations must be non-dimensionalized. This is achieved by using the substitutions

$$p = \frac{p^*}{p_r^* u_r^{*2}} \tag{14}$$

$$u = \frac{u^*}{u_r^*}$$

$$t = \frac{t^* u_r^*}{l_r^*}$$

$$\rho = \frac{\rho^*}{\rho_r^*}$$

$$x = \frac{x^*}{l_r^*}$$

where, as before, the asterisk represents a dimensional quantity, the subscript r denotes a reference value, and l is length. It is common to choose reference values that have physical significance. Examples include the chord of the wing of an aircraft for l_r^*, and the freestream velocity for u_r^*.

Using the variable substitutions given in Equations (14), the non-dimensional Navier-Stokes equations are

$$\frac{\partial \rho}{\partial t} + \frac{\partial (\rho u_i)}{\partial x_i} = 0\,, \tag{15}$$

$$\frac{\partial (\rho u_j)}{\partial t} + \frac{\partial\, (\rho u_j u_k)}{\partial x_k} = \frac{\partial}{\partial x_i}\left\{-\delta_{ij} p + \frac{\mu}{Re}\left[\left(\frac{\partial u_i}{\partial x_j} + \frac{\partial u_j}{\partial x_i}\right) - \delta_{ij}\frac{2}{3}\frac{\partial u_k}{\partial x_k}\right]\right\}, \tag{16}$$

$$\begin{aligned}\frac{\partial}{\partial t}\left(\frac{p}{\gamma - 1} + \frac{1}{2}\rho u_j u_j\right) + \frac{\partial}{\partial x_k}\left[\left(\frac{p}{\gamma - 1} + \frac{1}{2}\rho u_j u_j\right) u_k\right] \\ = \frac{\partial}{\partial x_i}\left\{u_j\left(-p\delta_{ij} + \frac{\mu}{Re}\left[\frac{\partial u_i}{\partial x_j} + \frac{\partial u_j}{\partial x_i} - \delta_{ij}\frac{2}{3}\frac{\partial u_k}{\partial x_k}\right]\right.\right. \\ \left.\left. + \frac{\mu}{(\gamma - 1) Pr\, M^2 Re}\delta_{ij}\frac{\partial T}{\partial x_j}\right)\right\}\end{aligned} \tag{17}$$

where γ is the specific heat at constant pressure divided by the specific heat at constant volume. To close these equations, the ideal gas law (Equation (4)) is non-dimensionalized using the same reference parameters, producing

$$p = \frac{\rho T}{\gamma M^2}. \tag{18}$$

There are three dimensionless coefficients that appear in these equations. The first dimensionless parameter is called the Mach number. This is given by

$$M = \frac{u_r^*}{a_r^*} \tag{19}$$

where a_r is the reference speed of sound. Next is the Prandtl number. It describes the ratio of the viscous diffusion rate to the thermal diffusion rate and is given by

$$Pr = \frac{c_p^* \mu^*}{k^*}. \tag{20}$$

In this expression, c_p^* is the specific heat of air at constant pressure and k is the thermal conductivity of air. The last dimensionless parameter is the Reynolds number which describes the ratio of inertial forces to viscous forces in the fluid. This parameter is given by

$$Re = \frac{\rho_r^* u_r^* l_r^*}{\mu_r^*}. \tag{21}$$

The Reynolds number is the similarity parameter of most interest for low speed wind tunnels (i.e. M < 0.3) [11].

Dimensional analysis of the governing equations of fluid mechanics shows that two flows will be similar if:

1) The bodies are geometrically similar (i.e., one is a scale model of the other)

2) The similarity parameters are the same for both flows

This is important because conducting experiments on scale models is one of the primary activities of wind tunnels. This means that full-scale behavior can be predicted based on experimental results if the non-dimensional flow parameters can be properly replicated in the wind tunnel. However, it is difficult to match both the Mach and Reynolds number in most cases, and many times neither can be matched perfectly. Decisions based on intuition and knowledge of the system being tested must be made regarding which parameter to more closely replicate and whether replicating them is necessary [11].

2.2.2. Basic Design Decisions

This section will highlight some of the important decisions involved with designing a low-speed wind tunnel and give examples of tunnels that exhibit common features.

It is common when designing a wind tunnel to first consider the desired test section size. The required size is determined by its intended application, laboratory size constraints, and budgetary constraints. A wide range of wind tunnels have been built based on these constraints. On the large end, the National Full-Scale Aerodynamics Complex at NASA Ames (see Figure 6) has two test sections. The smaller test section is 12.19 m (40 ft) by 24.38 m (80 ft) and can reach speeds up to 154.2 m/s (345 mph) and the larger test section is 24.38 m (80 ft) by 36.58 m (120 ft) and can reach speeds of 51.41 m/s (115 mph) [18]. The larger test section is big enough to fit a full-scale Boeing 737 in it. In contrast, it is not uncommon for educational wind tunnels to have test section diameters as small as 10 cm and be limited to speeds of less than 15 m/s [1]. For design purposes, a good rule of thumb is that model airplanes and airfoils should take up at most 80% the width of the test section. Furthermore, for test articles like airplanes, a width to height ratio of 1.5 is common. That said, it is advantageous for models to be small compared to the size of the test section , as this lowers the impact of the test section walls on the results [1]. For the same flow velocity, larger test sections allow larger objects to be tested and therefore a larger range of Reynolds numbers can be achieved. The required power and cost of tunnel building materials tend to vary with the test section hydraulic diameter squared [1], while the power consumption of the tunnel tends to increase with the test section airspeed cubed [19].

Figure 6. An aerial view of the National Full-scale Aerodynamics Complex. Image taken from Ref. [20].

The second design consideration to be made is if the tunnel is to be a return (closed circuit) or non-return (open circuit) type. Closed circuit wind tunnels are designed to pull air through a closed loop. Figure 7 is an example of a closed circuit tunnel as the air passes in a clockwise direction. Conversely, open circuit tunnels pull the air from the room through the test section and exhaust it back into the room. A schematic of the UC Davis Aeronautical Wind Tunnel Facility (AWT) is shown in Figure 8. This is an example of a standard open return wind tunnel. Most small research tunnels with test sections less than 0.61 m (2 ft) in diameter are open return [19], in part because of their lower construction costs. Open circuit wind tunnels are often less energy efficient, but energy operating costs for small wind tunnels tend to be relatively small to begin with [1]. Therefore, larger tunnels tend to be closed circuit with either one or two return paths. However, closed circuit tunnels are more expensive to construct and can be more difficult to design than open circuit tunnels. Because open circuit tunnels are open to the atmosphere at the settling chamber, the static pressure in the test section, where the air speed is the highest, is lower than atmospheric

pressure. This means that leaks in the test section are inevitable because holes are often drilled into the test section to install models or probes. Open circuit tunnels are also sensitive to obstructions in the room, such as furniture, other equipment or the walls. Placing an open return tunnel too close to a wall can have adverse effects on test section flow. Therefore, open return tunnels require a large room as to minimize this effect [19].

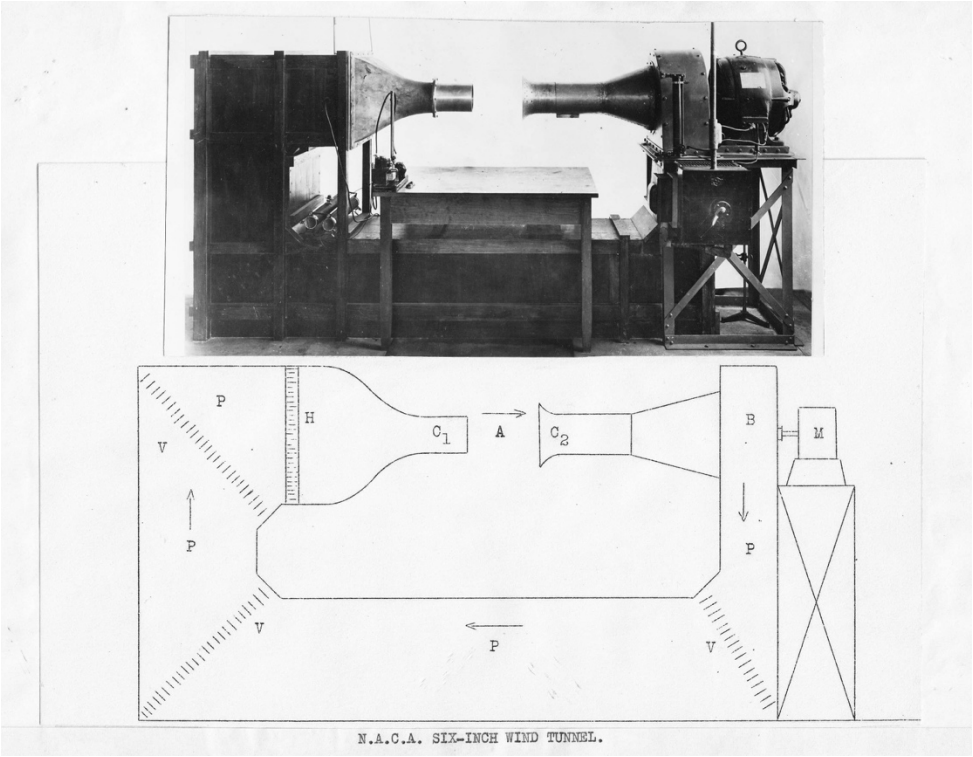

Figure 7. The NACA 6-inch tunnel is an example of an early open throat wind tunnel. Air is blown in a clockwise direction past the test section. Image taken from Ref. [21].

Another significant design decision is whether the test section itself is an open or closed type. An open test section is a test section that is not enclosed on all sides. Conversely, a closed test section is one which is closed on all sides. There are also hybrid and partially open test sections. Figure 7 is an example of an early wind tunnel with an open test section. There are some disadvantages for open test sections. First, open test section (open throat) tunnels do not work with open circuit tunnels that have a blower in the diffuser because the room can become too turbulent. This means that either the test section must be placed inside of a separate air-tight room or the tunnel must be closed return. Open throat tunnels

can also suffer from pulsations, the same way a pipe organ vibrates. If the object being tested creates a wake that is too big, the collector can interfere with the aerodynamics. However, open throat tunnels make it easier to change and work on test models, and make it easier to insert measurement probes. In general, closed throat wind tunnels have more advantages. However, several hybrid, partially open, convertible, or slotted wall wind tunnels have been made for use in the automotive industry and V/STOL development.

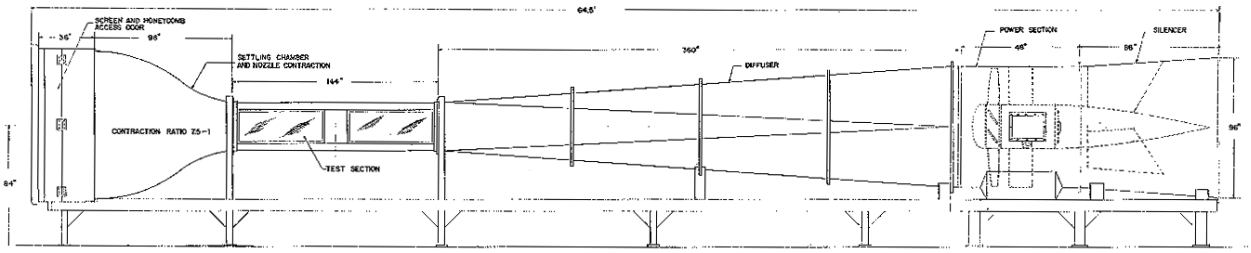

Figure 8. A schematic of the UC Davis Aeronautical Wind Tunnel Facility. This wind tunnel is an open-circuit design. Air enters the tunnel on the left, is contracted through a nozzle, passes through the test section, expands through a diffuser, passes the fan that powers the process, and exits the tunnel and returns to the room on the right side of the figure.

2.2.3. Section Loss and Power Considerations

To aid in the design of the Houghton College wind tunnel, a script was written in Octave (an open-source MATLAB alternative). This script has two primary purposes. The first is to calculate the dimensions of various components of the wind tunnel given constraints on selected components. The second purpose of this script is to estimate the required fan specifications needed to achieve a test section speed of 44.7 m/s (100 mph). This is done by calculating the stagnation pressure drop across each component as a function of its geometry, and the Reynolds number and Mach number for each component. This section will review the semi-empirical equations used to estimate these losses. It is important to note that these equations are quasi-one-dimensional. The cross-sectional area is allowed to change throughout the wind tunnel and the air speed is only a function of the cross-sectional area.

As mentioned in Section 2.1.3, inefficiencies can be thought of as a drop in stagnation pressure throughout the wind tunnel. Wattendorf [22] considers losses in a return-type wind tunnel by considering the losses of each component in succession. Eckert, Mort and

Jope [23] take the same approach and compare the estimations given by Wattendorf to several existing wind tunnels. A similar approach is taken here. The tunnel can be broken into constant area sections, corners, diffusers, contracting sections, etc. In each of these sections, apart from the fan, there are flow losses due to friction between the flowing gas and solid boundaries. The successive drops in total pressure for each component are balanced out by the pressure rise across the fan.

The power loss, or drop in stagnation pressure, of each section is modeled as being proportional to the dynamic pressure at the entrance of that section. For example, the drop in stagnation pressure for the i^{th} component of the wind tunnel is given by

$$\Delta p_{0_i} = K_i \frac{1}{2} \rho u_i^2 = K_i q_i \tag{22}$$

where q_i is the dynamic pressure at the entrance of the i^{th} component. K_i is called the pressure loss coefficient and can be estimated as a function of geometry of the i^{th} component and viscosity of the air. Then, the total efficiency of the wind tunnel is calculated as the ratio of the flow's kinetic energy in the test section to the energy dissipated in the tunnel due to friction. An expression for this energy ratio is

$$E_R = \frac{\frac{1}{2} \rho u_t^2}{\sum_i \Delta p_{0i}} = \frac{q_t}{\sum_i K_i \, q_i} \tag{23}$$

where the subscript t refers to the quantity as measured in the test section. Because both the numerator and denominator are effectively energy terms, both could also be considered as energy per unit time. This means that the power delivered by the fan must be at least q_t / E_R. It is important to note that this definition for the required fan power does not account for the electro-mechanical efficiency of the fan, but only the aerodynamic efficiency of the tunnel itself.

Given this definition of the energy ratio, it follows that estimating the loss coefficient, K_i, for each component of the tunnel is key to estimating the aerodynamic efficiency of the tunnel. Wattendorf [22] provides semi-empirical formulas for the loss coefficient of a variety of

wind tunnel components. These are summarized next, starting with the loss coefficient for a constant area section. This is given by

$$K_l = f\frac{L}{D_h} \tag{24}$$

where f is the friction coefficient, $D_h$is the hydraulic diameter, and L is the length of the component. The hydraulic diameter is a commonly used term when dealing with flow in rectangular ducts. It is defined as

$$D_h = \frac{2ab}{a+b} \tag{25}$$

where a and b are the width and height of the duct. The friction coefficient, f, is given by the Prandtl universal law of friction [22]

$$\frac{1}{\sqrt{f}} = 2\log_{10} Re\sqrt{f} - 0.8\,. \tag{26}$$

This loss coefficient is used for the test section and any other section where the cross-sectional area is constant.

When considering the loss coefficient for a diffuser, it is written in terms of the equivalent conical angle. This angle, as shown for a cone in Figure 9, is the angle of expansion. More generally, it can also be used for diffusers that do not have a circular cross section. In this case, the equivalent conical angle is the angle of expansion that would occur if the entrance and exit of the diffuser were circular and maintained the same cross-sectional area on each end as the actual diffuser. Mathematically this can be expressed as

$$\theta_e = \tan^{-1}\frac{\frac{1}{2}\left(\sqrt{A_R}-1\right)}{L/D_1} \tag{27}$$

where $A_R$is the ratio of the area of the larger side to the area of the smaller side, D_1 is the hydraulic diameter at the entrance, and L is the length of the diffuser.

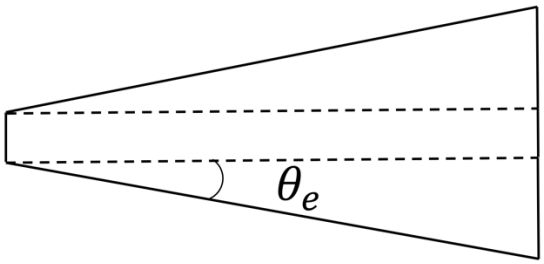

Figure 9. A depiction of the conical angle for a cone-shaped diffuser. The equivalent conical angle is the angle of expansion that would occur if the entrance and exit of the diffuser were circular and maintained the same cross-sectional area on each end as the actual diffuser.

One of assumptions made about diffuser losses is that the total loss can be broken into the sum of friction losses and expansion losses, as indicated by

$$K_d = K_f + K_{ex} \tag{28}$$

where

$$K_f = \left(1 - \frac{1}{A_R^2}\right)\left(\frac{f}{8\sin\theta_e}\right) \tag{29}$$

and

$$K_{ex} = K_{e(\theta)}\left(\frac{A_R - 1}{A_R}\right). \tag{30}$$

$K_e(\theta)$ is given by Eckert et al. [23] for diffusers with a square cross section

$$K_e(\theta) = \begin{cases} 0.09623 - 0.004152\theta \quad \text{for } 0 < \theta < 1.5° \\ 0.1222 - 0.04590\theta + 0.02203\theta^2 + 0.003269\theta^3 \\ -0.0006145\theta^4 - 0.00002800\theta^5 + 0.00002337\theta^6 \\ \text{for } 1.5° \le \theta \le 5° \\ -0.01322 + 0.05866\theta \quad \text{for } 5° < \theta\,. \end{cases} \tag{31}$$

Recommended practice is for diffusers to maintain an equivalent conical angle of 3° or less with a total area ratio of less than 3 [1]. In general, the risk of boundary layer separation increases with a larger equivalent conical angle and area ratio [24]. In some cases, diffusers with a more aggressive expansion are used. So-called wide-angle diffusers are used to increase the nozzle contraction ratio for a wind tunnel, which can improve overall flow quality in the test section. Barlow [1] states that these diffusers often have area ratios of 2-4 and 22.5° equivalent conical angles. While they can be used to increase test section air flow quality, they introduce additional losses and require screens to avoid boundary layer separation. A wide-angle diffuser is not used in the present design so further details are not included here. See Mehta [25] for more details on wide-angle diffuser design.

For closed circuit wind tunnels, corners are equipped with turning vanes to reduce losses and straighten the airflow after the corner. Figure 10 diagrams an example of a corner that uses cambered airfoil turning vanes. These vanes can vary in geometry and chord-to-gap ratio. Barlow [1] gives an estimation for the loss coefficient of a corner as

$$K_c = 0.10 + \frac{4.55}{(\log_{10} Re_c)^{2.58}} \tag{32}$$

where the Reynolds number is based on the turning vane chord length. Equation (32) is a conservative estimate and losses can often be reduced with careful design or increased with poor design. Consequently, the use of CFD for pressure loss estimates can be useful in choosing the airfoil shape, the chord length, and the gap-to-chord ratio. Equation (32) only includes chord length, limiting its predictive power.

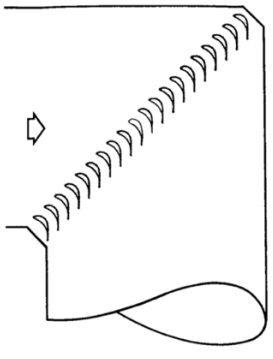

Figure 10. An example of cambered airfoil turning vanes in a corner. The flow direction is specified by the arrow. Diagram taken from Ref. [26].

The nozzle primarily serves two purposes. The first is to increase the mean air velocity before it enters the test section. This allows for the air speed in the rest of the tunnel to be lower relative to the test section. This is beneficial because the loss in each component tends to vary with the local flow speed squared. The second is that the total pressure remains close to constant across the contraction and, therefore, variations in velocity become smaller fractions of the average velocity at a given cross section. This means that less screens (discussed further below) are needed to reduce turbulence, therefore reducing pressure losses even more [27]. The loss coefficient for a nozzle is given by

$$K_{nt} = 0.32 f_{avg} \frac{L_n}{D_{ts}} \tag{33}$$

where L_n is the length of the nozzle and D_{ts} is the hydraulic diameter of the test section. In this case, f_{avg} can be found using Equation (26) based on the average of the Reynolds numbers at the entrance and exit of the nozzle. While the loss coefficient will also depend on the contraction shape, the effect of the exact shape of the contraction is relatively small because the losses for nozzles are typically on the order of 3% the total wind tunnel loss [1]. To properly design a nozzle, it is common to use computer simulations to check for boundary layer separation and optimize the flow uniformity at its exit – the start of the test section. See Mehta [27] for a more detailed approach to contraction geometry and separation predictions.

Screens and honeycombs are used to straighten the flow and increase flow uniformity immediatly before the nozzle. Eckert et al. [23] gives relations for screen loss coefficients which are based on the porosity. The porosity of a wire mesh is dependent on the wire diameter and weave density. If d_m is the wire density and w_m is the weave density, then the porosity is given by

$$\beta_s = \left(1 - \frac{d_w}{w_m}\right)^2 \tag{34}$$

and the screen solidity is

$$\sigma_s = 1 - \beta_s \,. \tag{35}$$

Typical porosity values for wind tunnel screens are between 0.5-0.8 [1]. The expression for the loss coefficient of a screen is given by

$$K_m = K_{\text{mesh}} K_{Rn} \sigma_s + \frac{\sigma_s^2}{\beta_s^2} \,. \tag{36}$$

Additionally, Idel'chik [28] gives a loss coefficient curve for screens as a function of the Reynolds number based on the wire diameter, Re_w. Barlow [1] provides a best-fit curve to this data

$$K_{Rn} = 0.785 \left(\frac{Re_w}{241} + 1.0 \right)^{-4} + 1.01 \,. \tag{37}$$

Idel'chik [28] gives the mesh factor, K_{mesh}, to be 1.0 for new metal wire, 1.3 for average circular metal wire and 2.1 for silk thread.

Eckert et al. [23] gives an expression for the loss coefficient for a honeycomb as

$$K_h = \lambda_h \left(\frac{L_h}{D_h} + 3 \right) \left(\frac{1}{\beta_h} \right)^2 + \left(\frac{1}{\beta_h} - 1 \right)^2 \tag{38}$$

where

$$\lambda_h = \begin{cases} 0.375 \left(\dfrac{\Delta}{D_h} \right)^{0.4} R_{e\Delta}^{-0.1} & \text{for } Re_\Delta \leq 275 \\ 0.214 \left(\dfrac{\Delta}{D_h} \right)^{0.4} & \text{for } Re_\Delta > 275 \end{cases} \,. \tag{39}$$

In these expressions, D_h is the hydraulic diameter of the honeycomb cell, β_h is the honeycomb porosity, Re_Δ is the Reynolds number based on the honeycomb material roughness and incoming flow speed, L_h is the honeycomb length in the flow direction, and Δ is the material roughness. Mehta and Bradshaw [29] suggest that about 25,000 total

cells in a honeycomb are sufficient for straightening the air flow. It should be noted that while the literature cited here discusses the loss coefficients for honeycombs, it is not clear how the roughness length, Δ, is defined. As a result, a constant guess of $K_h = 0.5$ was used for the pressure loss coefficient of the honeycomb in this study, as suggested by Barlow [1].

2.2.4. Fans and Drive Systems

The thrust of a fan and the drag in the various tunnel components varies with the fan angular velocity squared [1]. While smaller wind tunnels tend to only have angular velocity control, it is common in larger wind tunnels to control the fan blade pitch, too. However, having both is not essential. For controlling the fan angular velocity, most new facilities use variable-frequency drives for AC motors but some use solid-state controllers for DC motors, instead. In some cases, the motor is placed outside the wind tunnel with a shaft leading to the propeller, but this design is not essential. It is useful to mount motors onto anti-vibration mounts and connect them to the tunnel with flexible coupling to reduce vibrations [29]. It should also be noted that many wind tunnels have fan straighteners placed downwind of the fan to reduce swirl. Both Mehta [29] and Barlow [1] give more details on the power section of the wind tunnel.

2.2.5. Construction Requirements

When building wind tunnels, Barlow [1] suggests that components should be designed to withstand the maximum stagnation pressure with a safety factor of around 4. The structural strength of the wind tunnel is primarily to avoid vibration and to make sure that the motor will stay in place were the fan to lose half of its blades. Vibration contributes to noise and can, over time, reduce the structural integrity of the wind tunnel. For this reason, the support for various components should be stiffened until their natural frequency is well above the frequency of the fan [1].

Wind tunnels are made from a variety of materials including wood, plywood, thin or heavy metal, concrete, or plastic [1]. For small research and instructional tunnels, plywood is a good choice for the construction material. It allows for holes and chips to be easily patched and for the whole component to be replaced if need be. Plywood can be bolted together and

supported by wood or steel supports. The interior of the tunnel should be smoothed with corners and seams treated with caulking or a rubber gasket.

2.3. Measurement Techniques

The primary purpose of aerodynamic testing is to understand the flow field around an object. The flow field refers to the velocity vector, temperature, pressure, viscosity, and density as functions of position and time. This means that accurate results not only depend on the design of the tunnel itself, but also the techniques used to measure the flow field. One of the challenges associated with measuring the flow field around an object is that inserting an instrument into the flow field will almost inevitably disturb it. Designing and implementing minimally invasive measuring techniques can prove to be a challenge. Furthermore, obtaining accurate and precise flow field measurements with high time resolution requires careful design and planning. This section overviews some of the techniques used to obtain measurements.

2.3.1. Pressure Measurement

Measuring pressure is a vital component of wind tunnel testing. Pressure is defined as the normal force per unit area. In the context of aerodynamics, this force is exerted on an area element due to a time rate of change of momentum of the gas molecules impacting that surface [11]. Pressure is a function of both time and position.

One technique for measuring pressure is the manometer. The manometer is one the oldest devices for measuring differential pressure, or the pressure difference between two points, and is also one of the easiest to build. There are many different types of manometers but a simple one can be made by measuring the differences in height of a liquid sitting in a glass u-shaped tube with its two ends connected to the reference and tested points. This is called a u-tube manometer. See Figure 11 for an example. The difference in pressure is related to the height difference in the liquid by [1]

$$\Delta p = p_1 - p_2 = \Delta h \sin(\beta) g\left(\rho_f - \rho_a\right) \tag{40}$$

where Δh is the height difference of the liquid in the columns, β is the angle between the horizontal and the plane made by the two columns, g is the acceleration due to gravity, ρ_f is the density of the liquid in the tubes, and ρ_a is the density of the fluid in the wind tunnel.

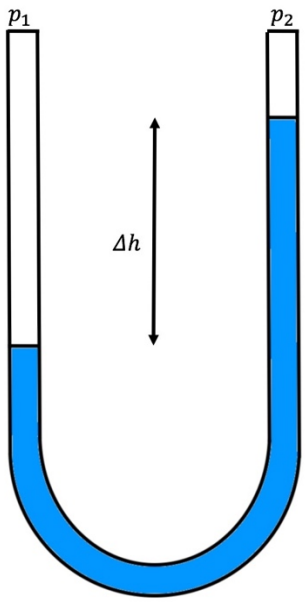

Figure 11. Simplified diagram of a u-tube manometer. The pressure difference between p_1 and p_2 can be found from the height difference of the fluid in the two tubes and density of both fluids.

Another way to measure pressure is using a pressure transducer. The term pressure transducer refers to devices that provide an electric potential or current in response to a pressure or change in pressure [1]. The most common pressure transducers are made from a small diaphragm that deforms when a pressure differential is introduced across it. The most common and inexpensive ways of measuring the deformation of the diaphragm include circuits that measure a change in capacitance or inductance due to the change in geometry. These types of pressure gauges can be made inexpensively and relatively small, but they do require periodic calibration. This means that a manometer or some other reliable pressure measuring technique is still required for calibrating pressure transducers in a wind tunnel.

It is important to note that there are a variety of other methods for measuring pressure that are not discussed in depth here. For example, some wind tunnels use pressure-sensitive paint which changes color when the pressure applied to it changes. See Gregory et al. [30] for a more comprehensive review of pressure-sensitive paints. Similarly, piezoelectric transducers produce an electric field in response to an applied pressure. See Barlow [1] for a more in depth look at pressure measurement methods.

2.3.2. Velocity Measurement

One of the most common ways to measure fluid velocity is using a pitot-static tube. Pitot-static tubes are an instrument which yield the difference between the total pressure and the static pressure of a moving fluid. The density of the fluid can be found using the equation of state based on a measured temperature and static pressure. This allows the velocity to be calculated. The principle of a pitot-static tube lies in Bernoulli's equation (see Section 2.1.3), which is a statement of conservation of energy. Solving Equation (12) for the velocity, gravitational effects can be neglected, giving

$$u = \sqrt{\frac{2(p_0 - p)}{\rho}} \ . \tag{41}$$

This instrument is made of two tubes, one inside the other, with one orifice facing the airflow and the second perpendicular to the air flow. An example pitot-static tube is given in Figure 12. As depicted, the orifice at A measures the total pressure, p_0, as it brings the air to a stop, and the orifice at B senses the static pressure, p, as the air moves past it. The pressures from the two orifices are connected to a manometer or pressure transducer and the pressure difference is approximately $\frac{1}{2}\rho u^2$. From this the velocity can be calculated using Equation (41).

The tip of a pitot-static tube can be either rounded or square. While square tipped tubes are more accurate at higher angles relative to the incoming flow [1], hemispherical tips offer less flow field disturbances further downstream near the second set of holes. However, tip-effect errors become negligent if the second set of holes is placed more than 5 or 6 tube diameters downstream from the base [31].

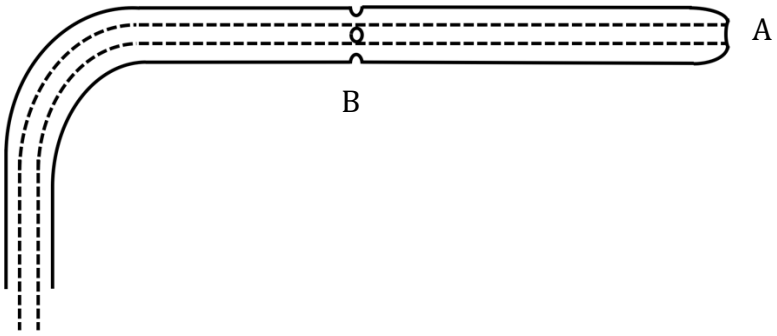

Figure 12. A simplified diagram of a pitot-static tube. The total pressure is measured at A as the air is brought to a stop going around the bend on the left. The static pressure is measured at B as the air moves past it. The velocity can be calculated based on the difference between these two pressures.

Another way to measure flow speed is thermal anemometry. This method takes advantage of the thermal and electrical properties of a thin wire or film. The faster air moves past this wire or film, the faster thermal energy will be transferred from it. This property can be used to measure the speed of the air.

To accomplish this, an electric current is passed through the wire or film to raise its temperature above the adiabatic recovery temperature of the gas [1]. Because the wire or film is not in thermal equilibrium with the fluid, energy is transferred to the fluid. The rate of energy transfer to the fluid is therefore a function of the air velocity. An electronic control system monitors the temperature of the wire, which is a function of its resistance, and adjusts the power in order to maintain a constant temperature in the wire. The airspeed, therefore, is a function of the power provided by the control system. When properly calibrated, accurate velocity measurements can be obtained with frequency responses of up to 50 kHz [32]. This makes thermal anemometry ideal for measuring velocities in turbulent flow fields.

Hot-wire sensors use a thin metal wire, with a typical diameter of 0.5 – 5 μm and a typical length of 0.1-1 mm. The wire is often composed of platinum or tungsten, or, less commonly, platinum-rhodium or iridium. Hot-film sensors are made of a thin platinum film deposited

onto a quartz support with another layer of quartz on top to reduce electromechanical effects. Hot-films are more commonly used in liquids while hot-wires are more commonly used in gases [32]. Furthermore, for hot-wires, single probes can contain multiple wires, which can be used for resolving flow direction as well as velocity.

Due to the development of the digital camera, particle image velocimetry (PIV) has become a viable way to measure the vector velocity of a flow field [33]. This is accomplished by introducing tracing particles to the air and measuring their velocity as they follow the flow. The tracing particles need to be small enough to properly follow the air. The particles are then illuminated and two images of the particles are captured. The velocity of the particles, and therefore the fluid, can be calculated from the average displacement of the particles within an interrogation window and the time between the two frames. This results in a vector field of the fluid flow at the resolution of the chosen interrogation window size. PIV systems are commonly used for two-dimensional flow field resolutions, but three-dimensional flow fields can be resolved with the use of two cameras [34]. Liu and Katz [35] used a four-exposure PIV system to measure acceleration of a flow field. From this they could calculate the pressure distribution of the test section. PIV software is available both commercially and though open-source options. OpenPIV is one such open-source option and there are versions for Matlab, Python and C++ [36].

Chapter 3

DESIGN CONSIDERATIONS AND METHODOLOGY

3.1. Basic Design Decisions

Now that the theory and background information on wind tunnel design have been presented, a discussion on the design methodology used for this project will be given. First, general wind tunnel layout decisions will be discussed. Then the procedure used to determine the dimensions of the wind tunnel is given followed by the loss coefficient estimates calculated based on this geometry. Lastly, a review of the current progress made on the design, construction, and purchasing of needed materials is given.

As mentioned in Section 2.2.2, most wind tunnels with a test section hydraulic diameter of less than 0.61 m (2 ft) are of the open return type. While the exact size of the test section was later calculated from geometric and power efficiency constraints, it was apparent from the beginning of the design process that the test section for the Houghton College wind tunnel would be less than 0.61 m in diameter. However, due to the small size of the laboratory, an open return tunnel would be impractical. Effects from the ends of the tunnel being too close to the walls of the room would sharply reduce efficiency, lowering test section speeds. Another consideration is that open-return tunnels are louder than similarly-sized closed-return tunnels. Sound levels are made even more important here because of the small laboratory space and its proximity to classrooms and offices. As a result, a closed return design was selected. Figure 13 is a schematic for a general closed-return tunnel.

After deciding upon a closed type return, it was decided that including a wide-angle diffuser (discussed in Section 2.2.3) was not beneficial to the overall design of the wind tunnel. Wide-angle diffusers are placed upstream of the settling chamber. They are designed to slow the air down before passing it through the honeycombs and screens. They also allow for a larger nozzle area ratio which, in turn, creates a more uniform flow field in the test section.

The aforementioned code was used to calculate the size of various components of the wind tunnel given area ratio constraints on the wide-angle area ratio, nozzle area ratio, first diffuser area ratio, diffuser angle and a total length of 4.72 m (15.5 ft). After testing several different combinations of these parameters, it became apparent that the desired test section size and speeds would not be possible if a wide-angle diffuser was included.

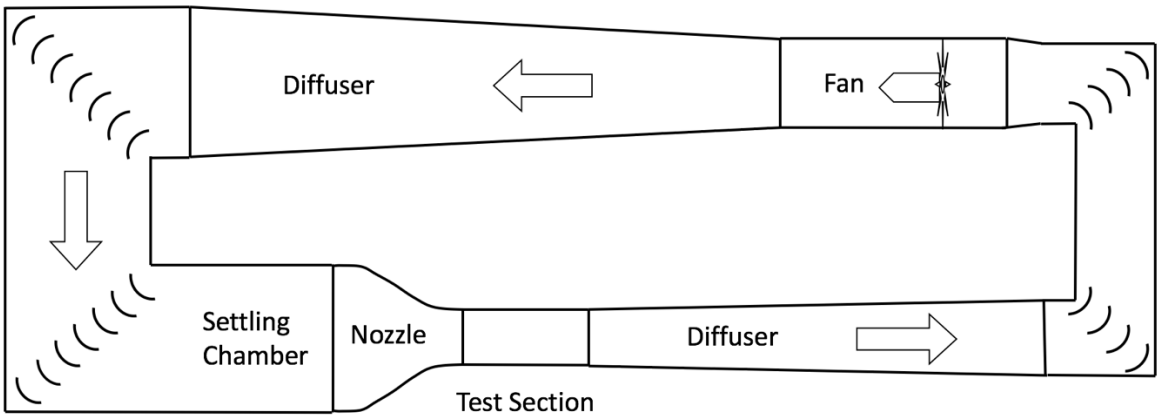

Figure 13. Schematic of the overall wind tunnel design that highlights the most important components.

3.2. Constraints, Methodology, and Design

In this section, specific constraints imposed on the wind tunnel design are discussed. Then the overall design methodology is described as are the details of the chosen design.

The first constraint that was imposed on the design process was a test section velocity of 44.7 m/s (100 mph). Smaller speeds would not be ideal for accomplishing the types of tests the physics department at Houghton College hopes to do with this tunnel. Specifically, lower speeds would further limit the range of Reynolds numbers that could be achieved. The second constraint placed on the design of the wind tunnel is the area ratio of the nozzle. It is ideal to maximize this value because it will cause the air in the rest of the tunnel to move slower relative to the air in the test section. Because the losses of each component vary with the localized air speed squared, maximizing this value will increase the efficiency of the tunnel. This means that a nozzle ratio of as close to 6 as possible was desired (based on a suggestion from Mehta [29]). However, the specific design of the contraction requires

computational analysis to optimize the flow uniformity and pressure loss. See Brassard et al [37], Fang [38], Fang et al. [39], Leifsson [40], Mikhail [41], and Mehta and Bell [27] for work on specific contraction designs.

Ultimately a nozzle area ratio of 5.45 and an area ratio of 3 for the first diffuser were selected. This was done using code that iterated though various nozzle ratios from 5 to 6 by 0.05 and various diffuser angles 2° to 3° by 0.05°. A length by diameter ratio of 2.5 for the test section, 0.8 for the nozzle, and 0.5 for the setting chamber were chosen based on a suggestion given by Barlow [1]. The resulting test section size and required fan specifications needed to achieve the desired test section speed were printed to a text file. Prior to this refining process, a fan had been purchased and only nozzle and diffuser area ratios that allowed the fan to fit were considered. More details on the purchased fan will be given in Chapter 4. The equations given in Section 2.2.3 were used to calculate the pressure loss coefficients for each section. As mentioned before, these coefficients have been non-dimensionalized by dividing the pressure loss in each section by the dynamic pressure of the test section.

Based on the chosen nozzle area ratio, all remaining geometric dimensions are calculated by the code and presented in Table 1. Figure 14 illustrates a sketch of the inside dimensions of the proposed wind tunnel. Air will move counter clockwise through the loop. The script also computes the loss coefficient, pressure loss, and air speed for each component, given in Table 2. It should be noted that the first diffuser is the section with the highest losses. This makes sense, not only because it is the longest component, but it has the second highest air speed, behind the test section. Note that corners, although not estimated to make a large contribution to the overall losses, have much larger losses if they are not designed and built properly. Because the nozzle makes up only two percent of the total losses, the primary goal of its subsequent detailed design should be maximizing flow uniformity. Maximizing the efficiency of the nozzle is not a concern when its losses are small to begin with.

For the purpose of estimating required fan characteristics, the energy ratio (E_r) is calculated using Equation (23). Its value is 2.60 which means that the wind tunnel requires

1.73 kW to be added by the fan to reach test section speeds of 44.7 m/s (100 mph). This is equivalent to 2.32 hp. Given the size of the test section, the fan would need to displace 3.84 m^3s^{-1} (8,130 $ft^3 min^{-1}$) of air and have a total pressure rise of 452 Pa (1.82 in. of water). The acquired fan (described in the next section) is capable of meeting these operational requirements.

3.3. Current Progress

Many of the required materials and components of the wind tunnel have been purchased. See Table 3 for a list of all purchased items along with their cost, distributor and manufacturer. This includes 19.1 mm (¾ in.) medium density overlay (MDO) plywood and 13 mm (½ in.) acrylic needed to build the wind tunnel. MDO plywood's primary use is building concrete molds. This means that it has excellence structural stability and one side that is smoothed. These characteristics are ideal for building our wind tunnel because the air pressure inside the tunnel will be above atmospheric and the smoothness will reduce friction. Furthermore, one side of the tunnel will be constructed out of acrylic so that air flow throughout the tunnel can be visualized and important tunnel components can be seen. In addition, a steel frame has been constructed out of Unistrut to support the wind tunnel once it is complete. (Figure 15). Unistrut was selected as a building material because of its adjustability. The bolts which hold the joints together can be loosened and the horizontal bars can be moved, allowing the tunnel to be placed as to match the height of the fan.

For the fan, a vane axial fan manufactured by New York Blower (Figure 16) was selected to meet the requirements covered in Section 3.2. This fan is 53.3 cm (21 in.) in diameter with nine blades pitched at 33.0°. It has a 5.6 kW (7.5 hp) motor and can spin at a maximum of 3500 rpm. Because it has a circular cross section, two custom-made transitions (Figure 17) have been fabricated by Nordfab to be used to convert from a circular cross section to a square cross section. The fan was selected to match cross sectional area with the components before and after it as closely as possible. The fan is driven by a variable frequency drive (VFD) that has been purchased and installed in the laboratory. A C10 Customizable Vector AC Drive VFD made by Saftronics was selected to drive the fan.

Table 1. A list of the dimensions of each component of the tunnel. This list starts at the test section and works downstream from there. Note that for the purpose of estimating losses, the motor and transitions between square and circular cross section were modeled as a constant area section with a loss coefficient calculated using Equation (24).

Component	Upstream Width (cm)	Upstream Height (cm)	Downstream Width (cm)	Downstream Height (cm)	Length (cm)
Test Section	35.9	23.9	35.9	23.9	73.3
Diffuser 1	35.9	23.9	49.5	49.5	192.4
Corner 1	49.5	49.5	49.5	49.5	49.5
Edge 1	49.5	49.5	49.5	49.5	45.6
Corner 2	49.5	49.5	49.5	49.5	49.5
Fan	49.5	49.5	49.5	49.5	173.9
Diffuser 2	49.5	49.5	68.4	68.4	180.7
Corner 3	68.4	68.4	68.4	68.4	68.4
Edge 2	68.4	68.4	68.4	68.4	30.5
Corner 4	68.4	68.4	68.4	68.4	68.4
Settling Chamber	68.4	68.4	68.4	68.4	34.2
Nozzle	68.4	68.4	35.9	23.9	54.7

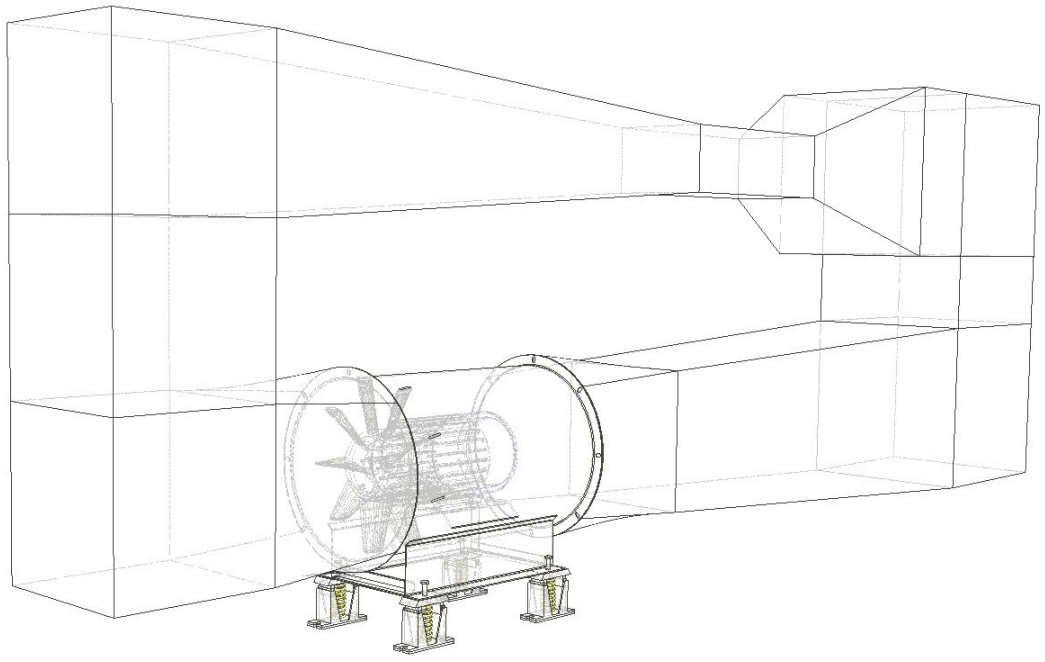

Figure 14. A sketch of the inside dimensions of the wind tunnel. The air will pass counter clockwise through the loop. Note that a detailed design for the nozzle has not been completed. The nozzle shown here uses straight walls to connect the settling chamber upstream and the test section downstream.

Figure 15. The steel frame constructed out of Unistrut to support the wind tunnel when complete. The acquired vane axial fan from New York Blower is also visible.

Table 2. A table of the estimated loss coefficient, stagnation pressure loss, percentage of total losses and velocity for each component of the wind tunnel. The list starts with the test section and precedes counter-clockwise as shown in Figure 13.

Component	**Loss Coefficient**	**Stagnation pressure Loss (Pa)**	**Loss Percentage**	**Velocity (m/s)**
Test Section	3.07e-2	36.2	7.8	44.70
Diffuser 1	1.23e-1	144	31.3	44.70
Safety Screen	6.51e-2	76.6	16.6	15.69
Corner 1	2.13e-2	25.0	5.4	15.69
Edge 1	1.66e-3	1.95	0.4	15.69
Corner 2	2.13e-2	25.0	5.4	15.69
Fan	5.82e-3	6.84	1.5	15.69
Diffuser 2	9.30e-3	10.9	2.4	15.69
Corner 3	6.22e-3	7.26	1.6	8.20
Edge 2	2.14e-4	0.252	<0.1	8.20
Corner 4	6.22e-3	7.32	1.6	8.20
Settling Chamber	2.40e-4	0.283	<0.1	8.20
Honey Comb	1.68e-2	19.8	4.3	8.20
Screen	7.63e-2	89.8	19.5	8.20
Nozzle	7.80e-3	9.17	2.0	8.20

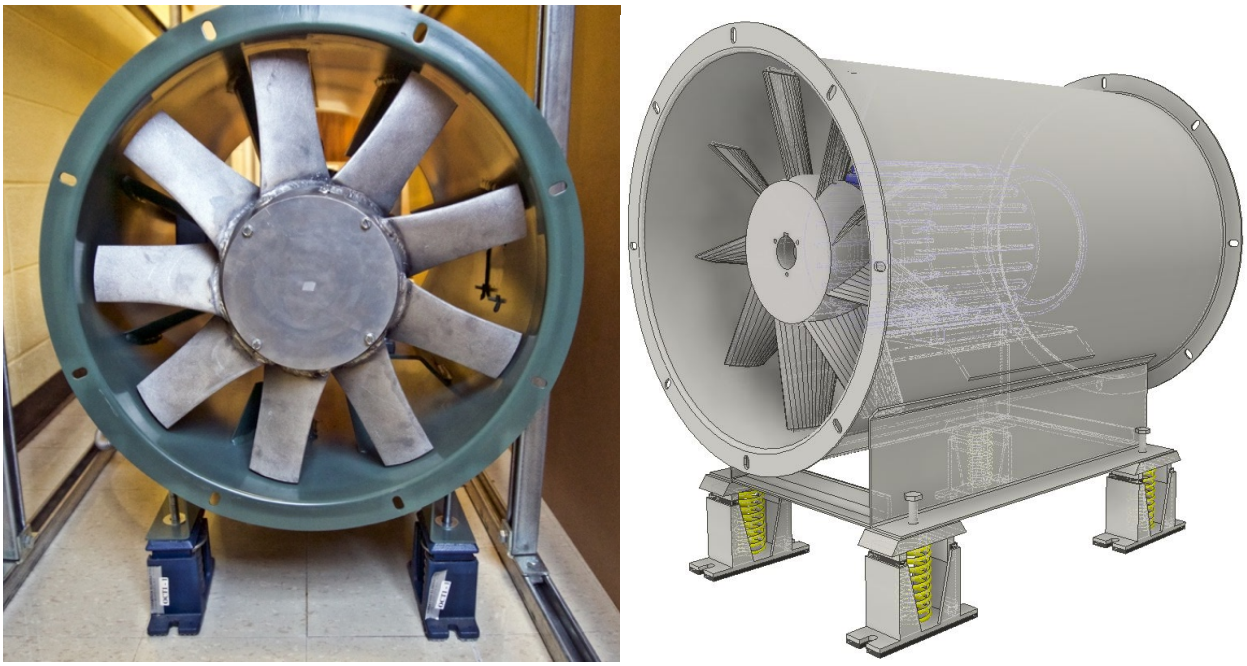

Figure 16. A photo of the fan (left) and a CAD drawing of the fan (right).

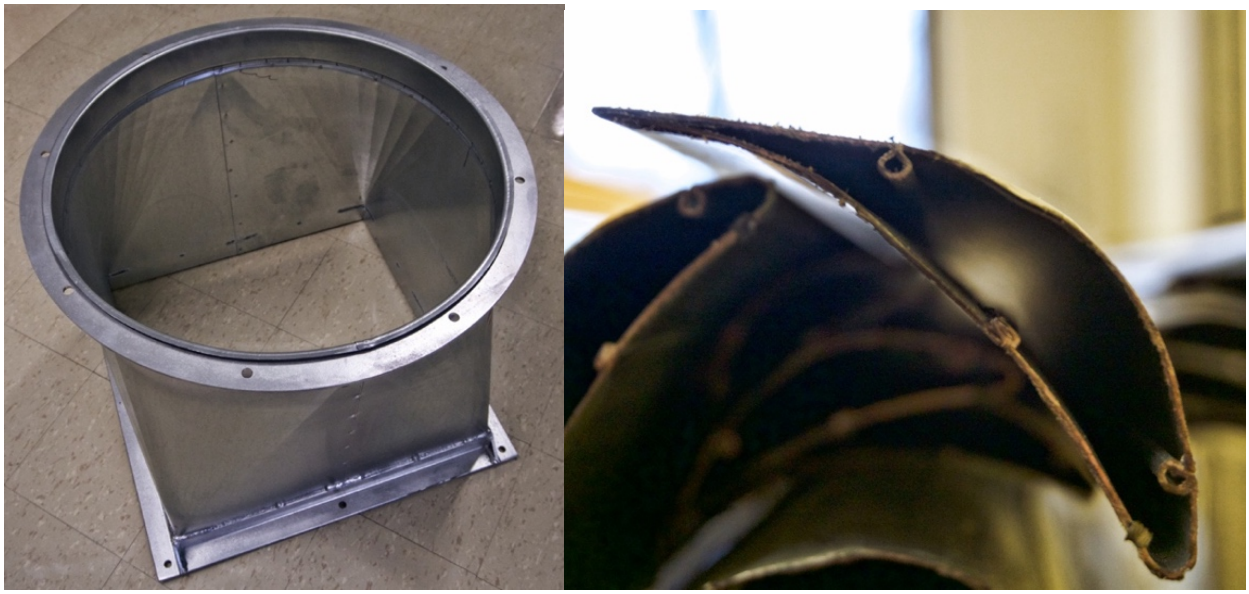

Figure 17. Custom-made sheet metal component for transitioning between square and circular cross sections (left) and sheet metal turning vanes for corners. (right).

A variety of other products have been acquired for the wind tunnel also. Turning vanes (Figure 17) were ordered from Aero Dyne to be installed in the corners. These will reduce losses as the air passes around the corners. A honeycomb sheet was ordered from Plascore, Inc. as well as screens from W.S. Tyler. A safety screen was purchased from Metals Depot to be placed after the first diffuser. This screen will help to stop anything that comes loose in the test section from entering the fan.

Table 3. A list of the materials purchased so far along with a price and product details.

TUNNEL COMPONENTS				
Price	**Shipping**	**Purchased From**	**Manufacturer (if different)**	**Item**
$1168.31	$149.95	Professional plastics		½" thick clear cast acrylic paper-masked sheet @ +/- 0.125" cut tolerance
$588.87		VFDs.com	Saftronics	C10 2007-1, AC Vector Drive VFD
$2,409.00	$172.00	Advanced Air, Inc.	New York Blower	Vaneaxial, 21" Diameter, Arrangement 4M, 33 degree blade pitch. Comes with a 7.5 HP motor with a maximum speed of 3600 RPM.
$498.53	$199.80	Lord and Sons, Inc.	Atkore International, Inc.	Unistrut and various connections
$508.00	$100.00	Aero Dyne		H-E-P Vane, 200 feet
$62.50	$13.46	Plascore, Inc.		PC2-250B2.000-13, 27"x27", 2" thick, 1/4" cell, honeycomb.
$407.79	$-	Belmont Hardware		8 Single-Sided, 3/4" sheets of Medium Density Overlay (MDO), 2x4's
$117.92	$15.00	W.S. Tyler		4-27"x27" 0.009" diameter wire, 316SS fine mesh. These are 16-count mesh screens with 73.3% open area.
$49.84	$35.13	Metals Depot		20"x20" Welded Wire Steel Mesh, 1" x 1" cells with 0.118" diameter wire
$630.00	$203.63	AB Flow-tek	Nordfab Ducting	Custom duct square to circular transition: 19.5"x19.5" to 21.25" diameter, length = 18.25"
INSTRUMENTATION				
$70.50	$16.96	Dwyer, Inc.		2- MARK II M-700PA U-Tube Manometers
$270.00	$28.68	United Sensor	United Sensor	PCC-18-KL and PCC-8-KL pitot-static tubes
Total Products	**Total Shipping**	**TOTAL**		
$6,781.26	$934.61	$7,715.87		

Chapter 4

CONCLUSIONS AND FUTURE WORK

4.1. Conclusions

The purpose of this project was to design a general-purpose low-speed wind tunnel. Code was written in Octave to calculate the geometry of each component of the tunnel given a set of constraints and geometry choices. The area ratio of the nozzle and first diffuser were chosen to maximize the ratio of the test section air speed to the air speed in the rest of the tunnel. Because the energy losses in each component tend to vary with the local air speed squared, it is ideal to maximize the nozzle area ratio to increase the efficiency of the tunnel. The equivalent conical angle is constrained to reduce the chance of separation in the diffusers, which would greatly increase the pressure loss. Given the maximum size of the wind tunnel, the code iterates through nozzle and diffuser area ratios, calculating required sizes for each component and ensuring there is enough room for the selected fan.

For each component, the code calculates the loss coefficient using a semi-empirical equation. The loss coefficient is based strictly on the geometry of the component and the viscosity of the air. From this, the total efficiency of the wind tunnel is estimated. Based on preliminary analyses using the code, a fan was purchased providing sufficient capabilities for the present application. The wind tunnel and fan have been designed to achieve a test section speed of 44.7 m/s (100 mph) and detailed sizing information has been given. The proposed wind tunnel will be 4.72 m (15.5 ft) long and 1.67 m (5.49 ft) tall. The test section will be 0.239 m (9.42 in.) tall, 0.359 m (14.1 in.) wide and 0.733 m (28.8 in.) long. To date, many of the necessary components and materials for the tunnel have been purchased and detailed design work is in progress.

4.2. Future Work

In this section, immediate and more distant future work is discussed. In the immediate category, a detailed design and drawing of the wind tunnel is under way, based on the basic design outlined in this work. This will ensure that the plywood and acrylic will be cut to the correct

dimensions to ensure that each component has the correct interior dimensions of the air. Figure 18 is a preliminary version of this drawing, detailing the configuration of plywood and acrylic. After this drawing is complete, construction of the tunnel can commence, with the exception of the nozzle and corners. Currently, work is being done to simulate airflow through the nozzle to select a contraction design which maximizes flow field uniformity in the test section. Similarly, work is being done to simulate airflow through the corners of the wind tunnel. The goal of these simulations is to determine the optimal spacing of the turning vanes to reduce losses and maximize flow uniformity in the corners. After simulations on the corners and nozzle have yielded optimal designs, they can be built.

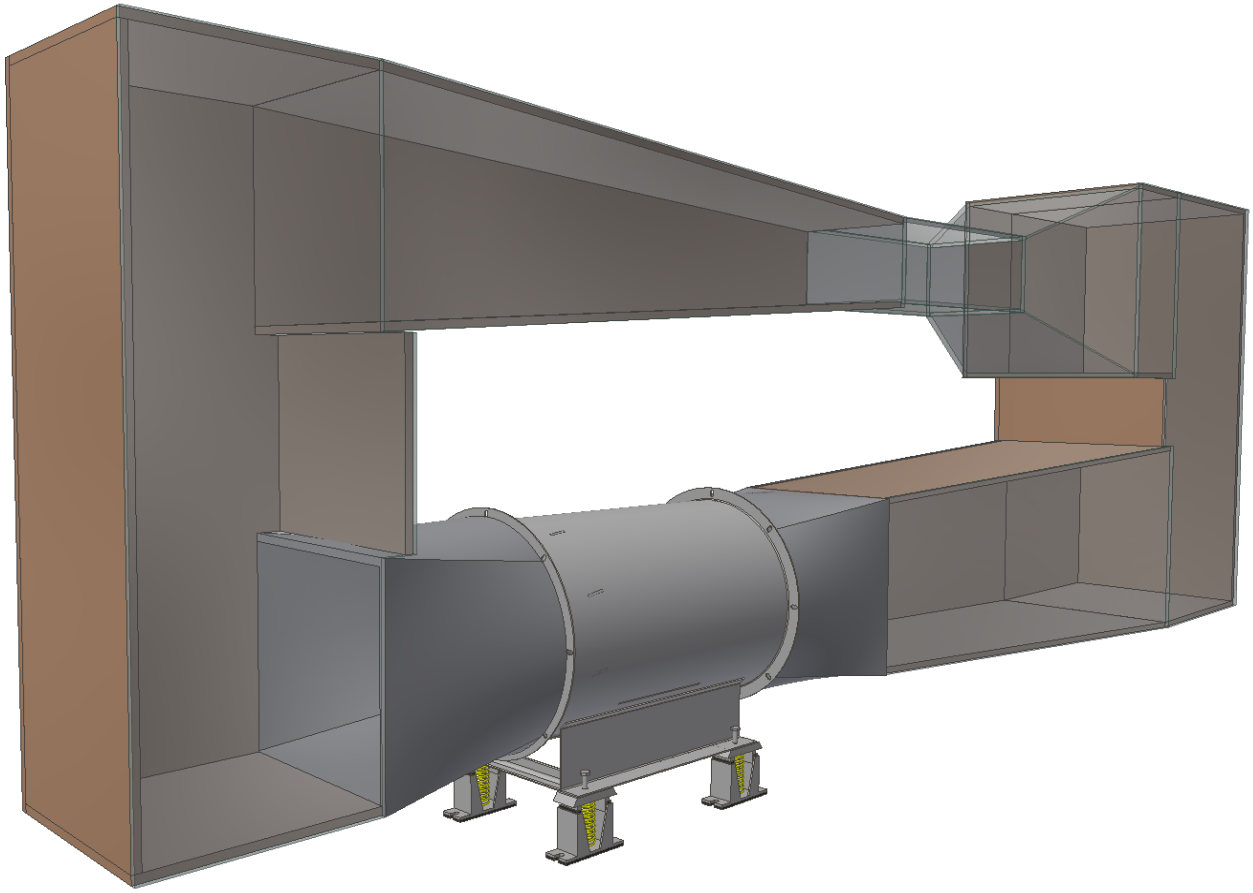

Figure 18. A preliminary diagram of the proposed wind tunnel.

In the more distant future, and once the construction of the wind tunnel is complete, instrumentation will need to be installed. This includes drilling holes to insert pitot-static tubes in the settling chamber and test section. Also, a balance for supporting and measuring forces on a

model (e.g. lift, drag) needs to be installed in the test section. After the instruments have been installed and calibrated, the tunnel can be used for experiments. A few options for experiments are listed next.

As mentioned in section 1.3, there are many examples of future research that could be conducted. One example is studying the effects of ice accretion on airplane wings. As ice builds up on airplane wings it can adversely affect drag and lift and, consequently, the flight of the plane. Our proposed wind tunnel is not capable of operating at freezing temperatures, but results from NASA Glenn could be used to help us study this problem. The Icing Research Tunnel at NASA Glenn can operate with air temperatures below freezing [42]. Water vapor is then injected into the tunnel and ice begins to build up on the model they are testing. Researchers at NASA Glenn scan the ice buildup to make a 3-d digital model. Figure 19 is a picture of a model with ice buildup and its corresponding 3-d model. These models can be replicated with a 3-d printer and tested in the Houghton College wind tunnel.

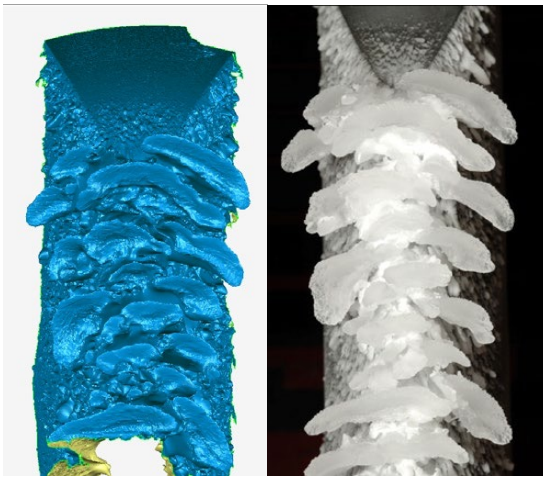

Figure 19. Researchers at NASA Glenn can produce 3-d scans (left) of ice accretion on airfoils that have been produced in the Icing Research Tunnel (right). Images take from Ref. [42].

A second example of possible future research is plasma actuation. Plasma actuation is a technique for actively controlling airflow, e.g., around an airfoil. Airfoils at a high angle of attack are at risk for separation to occur. Separation is when the boundary layer becomes detached from the surface of an object. For aircraft, separation on the wings is referred to as stall. When stall occurs, there is a rapid loss in lift and increase in drag. This can be seen

in the top image of Figure 20. Plasma actuators use a pair of electrodes with a high potential difference between them (3-12kV) at the front and middle of an airfoil to ionize the air as it passes over the front edge of the airfoil. This attracts the ionized air to the surface of the airfoil to reduce the chance of separation [43]. The bottom of Figure 20 demonstrates active control of air flow around an airfoil.

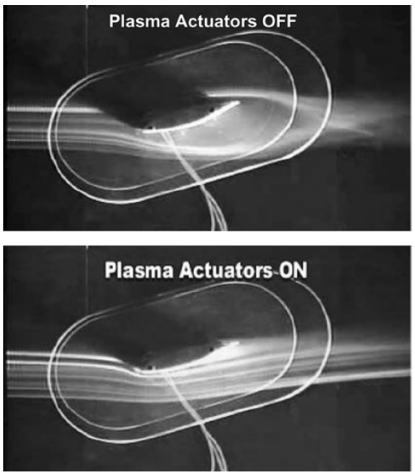

Figure 20. A demonstration of a plasma actuator actively controlling the air flow around an airfoil. Smoke is being used to visualize the flowfield and clearly shows separation when the actuators are off (top). The flow smoothly follows the airfoil surface when they are on (bottom). Image take from Post and Corke [43].

Lastly, the Houghton College low-speed wind tunnel will be used for teaching applications in the future. Specifically, it will be used in the context of an undergraduate fluid mechanics course. This can be useful in helping students understand fundamental fluid phenomena and measurement methodologies. For example, Reynolds [44] suggests a lab for undergraduates that focuses on plotting the lift of an airfoil as a function of air speed. Undergraduate wind tunnel labs are useful for both physics and engineering students, as well as non-technical students interested in aviation.

R e f e r e n c e s

[1] J. Barlow, W. Rae and A. Pope, *Low-Speed Wind Tunnel Testing*, 3rd ed. (Wiley-Interscience, New York, 1999).
[2] D. Anderson, R. H. Pletcher and J. C. Tannehill, *Computational Fluid Mechanics and Heat Transfer*, 2nd ed. (Taylor & Francis, 1997), pp. 5-55.
[3] P. Cusdin and J.D. Muller, Report QUB-SAE-03-01d, Queen's University, 2003 (unpublished).
[4] D. R. Chapman, AIAA Journal **17** (12), 1293 (1979).
[5] E. M. Kraft, ITEA **31** (3), 329 (2010).
[6] S. Chen, D. D. Holm, L. G. Margolin and R. Zhang, Physica D: Nonlinear Phenomena **133** (1), 66 (1999).
[7] C. Wagner, T. Huttl and P. Sagaut, *Large-Eddy Simulation For Acoustics*, 1st ed. (Cambridge University Press, 2007), pp. 89-91.
[8] M.R. Melanson, Paper No. 830 presented at the 46th AIAA Aerospace Sciences Meeting and Exhibit, Reno, NV, 2008 (unpublished).
[9] H. C. Garner, E. W. E. Rogers, W. E. A. Acum, and E. C. Maskell, NATO Advisory Group for Aerospace Research and Development Report No. AD657092, 1966 (unpublished).
[10] D. D. Baals and W. R. Corliss, *Wind Tunnels of NASA*, 1st ed. (Scientific and Technical Information Branch, National Aeronautics and Space Administration, Washington, D.C., 1981).
[11] J. D. Anderson, *Fundamentals of Aerodynamics*, 1st ed. (McGraw-Hill, Boston, 2001).
[12] O. Reynolds, Proceedings of The Royal Society of London **35** (224), 84 (1883).
[13] B. D. Steele, Technology And Culture **35** (2), 348 (1994).
[14] E. N. Jacobs and I. H. Abbot, NACA Report No. 416 (1932).
[15] J. V. Kirk, B. K. Hodder and L. P. Hall, NASA TN D-4233 (1867).
[16] I. G. Currie, *Fundamental Mechanics of Fluids*, 3rd ed. (CRC Press, Boca Raton, 2002).
[17] E. Buckingham, Physical Review **4** (4), 345 (1914).
[18] P. T. Zell, NASA TM 103920 (1993).
[19] P. Bradshaw and R. C. Pankhurst, Progress in Aerospace Sciences **5**, 1 (1964).
[20] "An aerial view of the National Full-scale Aerodynamics Complex" [Online]. NASA. https://www.nasa.gov/content/national-full-scale-aerodynamics-complex-nfac
[21] "6-inch Wind Tunnel" [Online]. NASA. https://crgis.ndc.nasa.gov/historic/NACA_Tunnel_One
[22]F. L. Wattendorf, *Proceedings of the Fifth International Congress for Applied Mechanics*, (1938), pp. 526-530.
[23] W. T. Eckert, K. W. Mort and J. Jope, NASA TN D-8243 (1976).
[24] J. M. Robertson and H. R. Fraser, Journal of Basic Engineering **82** (1), 201 (1960).
[25] R. D. Mehta, Progress in Aerospace Sciences **18**, 55 (1977).
[26] T. F. Gelder, R. D. Moore, J. M. Sanz and E. R. McFarland, NASA TM 87146 (1986).
[27] J. H. Bell and R. D. Mehta, NASA CR 17488 (1988).
[28] I. E. Idel'chik, *Handbook of Hydraulic Resistance*, 1st ed. (The Israel Program for Scientific Translation, Tel Aviv, 1966).

[29] R. D. Mehta and P. Bradshaw, The Aeronautical Journal of The Royal Aeronautical Society **83** (826), 443 (1979).
[30] J. W. Gregory, K. Asai, M. Kameda, T. Liu and J. P. Sullivan, Proceedings of The Institution Of Mechanical Engineers, Part G: Journal Of Aerospace Engineering **222** (2), 249 (2008).
[31] K. G. Merriam and E. R. Spaulding, NACA TN 546 (1935).
[32] G. Comte-Bellot, Annual Review Of Fluid Mechanics **8** (1), 209 (1976).
[33] A. Melling, Meas. Sci. Technol. **8** (12), 1406 (1997).
[34] M. S. Iliescu, G.D. Ciocan, and F. Avellan, Proceedings of the ASME 2002 Joint U.S.-European Fluids Engineering Division Conference, (2002), pp. 311-316.
[35] X. Liu and J. Katz, Experiments in Fluids **41** (2), 227 (2006).
[36] Z. J. Taylor, R. Gurka, G. A. Kopp, A. Liberzon**,** IEEE Transactions on Intrumentation and Measurement, **59** (12), 3262 (2010). See also http://www.openpiv.net
[37] D. Brassard and M. Ferchichi, Journal of Fluids Engineering **127**(1), 183-185 (2005).
[38] F. M. Fang, Journal of Fluids Engineering **119** (2), 454 (1997).
[39] F. M. Fang, J. C. Chen and Y. T. Hong, Journal of Wind Engineering and Industrial Aerodynamics **89** (3), 247 (2001).
[40] L. Leifsson and S. Koziel, Journal of Computational Science **7**, 1 (2015).
[41] M. N. Mikhail, AIAA Journal **17** (5), 471 (1979).
[42] S. Lee, A. Broeren, H. Addy, R. Sills and E. Pifer, NASA TM 217702 (2012).
[43] M. L. Post and T. C. Corke, AIAA Journal **42** (11), 2177 (2004).
[44] R. S. Reynolds, Journal of Aviation/Aerospace Education & Research **14** (2), 9 (2005).